https://doi.org/10.5194/egusphere-2024-1010
Preprint. Discussion started: 15 May 2024

Measurement report: The promotion of low-level jet and thermal-effect on development of deep convective boundary layer at the southern edge of the Taklimakan Desert

Lian Su[1], Chunsong Lu[2,3], Jinlong Yuan[2,3], Xiaofei Wang[4], Qing He[5], Haiyun Xia[1,2,3,*]

[1]School of Earth and Space Science, University of Science and Technology of China, Hefei 230026, China
[2]School of Atmospheric Physics, Nanjing University of Information Science and Technology, Nanjing 210044, China
[3]Collaborative Innovation Center on Forecast and Evaluation of Meteorological Disasters, Key Laboratory for Aerosol-Cloud-Precipitation of China Meteorological Administration, Key Laboratory of Meteorological Disaster of Ministry of Education, NUIST, Nanjing 210044, China
[4]Xinjiang Uygur Autonomous Region Meteorological Service, Urumqi 830002, China
[5]Institute of Desert Meteorology, China Meteorological Administration, Urumqi 830002, China

Correspondence to: Haiyun Xia (hsia@ustc.edu.cn)

Abstract. A vigorous development process of the deep convective boundary layer (CBL) was observed at the southern edge of the Taklimakan Desert on 6 June, 2022. Based on coherent Doppler wind lidar and ERA5 data, the formation mechanism of the deep CBL exceeding 5 km was well analyzed, which was mainly promoted by the low-level jet (LLJ) and thermal-effect. The LLJ has made sufficient momentum, energy and material preparations for the development of the deep CBL. Firstly, the cold downhill airflow of the Tibet Plateau leading to LLJ weakens the height and intensity of the temperature inversion layer, which reduces the energy demand for the broken of the IL. Secondly, the LLJ not only supplements the material and energy in the residual layer, but also suppresses the exchange with the lower atmosphere. In addition, the LLJ provides a driving force for the development of the deep CBL. In terms of thermal factors, the Tibet Plateau sensible heat driven air-pump and cold front transit provide additional impetus for the development of the deep CBL. Finally, the formation of deep CBL was catalyzed by the extreme thermal effects of the underlying surface, such as the furnace effect and the atmospheric superadiabatic expansion process. The study of the development of the deep CBL is important for revealing the land-air exchange process of momentum, energy, and material between the Taklimakan Desert and the Tibetan Plateau.

https://doi.org/10.5194/egusphere-2024-1010
Preprint. Discussion started: 15 May 2024

1 Introduction

The atmospheric boundary layer (ABL) is the place where the earth's surface exchanges momentum, energy and material with the free atmosphere (Stull, 1988; Garratt, 1994). The boundary layer height (BLH) is an important meteorological reference variable in the vertical direction, which indicates the atmospheric environmental capacity of the region and the vertical diffusion degree of pollutants (Holtslag and Boville, 1993). The study of the temporal and spatial distribution of BLH, which is closely related to human life, plays an important auxiliary role in monitoring air pollution and formulating pollution control policies according to local conditions.

The convective boundary layer (CBL) belongs to an unstable ABL, and the height of CBL should usually be lower than 2-3 km. However, under certain conditions, such as arid region and monsoon climate, the height of CBL can continue to develop upward and may exceed 5 km (Garratt, 1994). At present, a large number of scholars have found and analyzed the deep CBL phenomenon in the subcontinent of India (Basha and Ratnam, 2009; Raman et al., 1990), Sahara desert (Birch et al., 2012; Marsham et al., 2008), Mongolia (Han et al., 2015), Tibet Plateau (Che and Zhao, 2021; Lai et al., 2023), Badain Jaran Desert (Han et al., 2012), and Gobi desert (Zhang et al., 2002). The Taklimakan Desert (TD), which plays an important role in global climate change, has also carried out corresponding research work (Zhang et al., 2022; Wang et al., 2016; Wang et al., 2019). However, since the study site of MinFeng is located in the convergence area of the strong east-west airflows in the TD, resulting in the land-air interaction in this area is particularly prominent, so that the area is in bad wind-sand activity all the year round (Yang et al., 2016; Xiao et al., 2008). The unique geographical location and harsh climate of the study site, firstly, make the local representative ABL observation data relatively scarce. Secondly, the formation mechanism of the deep CBL is more complicated in this area. Finally, the formed deep CBL also has a profound impact on the supply of dust aerosol to the Tibetan Plateau (TP) (Jia et al., 2015; Meng et al., 2019).

When the experiment is carried out in the desert, the harsh desert climate environment will increase the performance requirements and the maintenance costs of meteorological equipment, thus increasing the difficulty of environmental monitoring. The coherent Doppler wind lidar (CDWL) needs to operate under the conditions of strict sealing and precise temperature control. In the detection of the ABL, the CDWL has the characteristics of low blind area, high radial spatial resolution and temporal resolution, long detection distance and little influence by ground clutter. These characteristics of CDWL enable it to carry out long-term continuous and stable detection in the desert areas, and make it one of the effective means to estimate the BLH in the desert (Li et al., 2017; Zhang et al., 2020; Collis, 1966; Zhang et al., 2021).

In this paper, the CDWL was used to conduct a long-term stable observation experiment in the MinFeng area of the TD, and a representative formation process of the deep CBL was observed on 6 June, 2022, local time (UTC+8). The CDWL data and ERA5 data were used to analyze the causes of the formation of the deep CBL. This paper is organized as follows: the study site, datasets and methods are described in Sect. 2. The CDWL observation results are presented and analyzed in Sect. 3. From the perspective of the whole desert region, the ERA5 reanalysis data were also analyzed in Sect. 4. Finally, a conclusion is drawn in Sect. 5.

https://doi.org/10.5194/egusphere-2024-1010
Preprint. Discussion started: 15 May 2024

2 Site, data resources, methods

2.1 Study site

The Taklimakan Desert (TD), is the second largest drifting desert in the world and the largest desert of China. Due to the blocking effect of the Tibet Plateau (TP) on the warm and humid airflow, the TD has become a typical extreme arid climate zone. The study site of MinFeng (37.06° N, 82.69° E, elevation 1418 m), located on the southern edge of TD and adjacent to the northern foot of Kunlun Mountains, which is significantly influenced by the TP. The area has the characteristics of long sunshine time, strong radiation, scarce precipitation, and the east-west airflows converge here, making it the most frequent place for wind-sand disasters in China. The average dust weather in this area exceeds 200 days per year, and the frequent wind-sand weather has a huge impact on human activities and health (Zhou et al., 2020; Zhou et al., 2022; Yang et al., 2016; Wu et al., 2016).

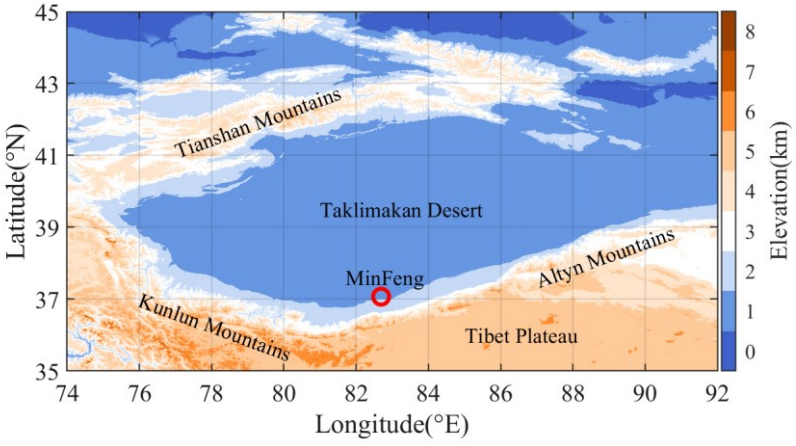

Figure 1. Elevation map of the Taklimakan Desert, and the study site of MinFeng.

2.2 Instruments and dataset

A compact CDWL working at eye-safe wavelength of 1.5 μm is used in this study. The pulse energy and repetition frequency of the laser are 130 μJ and 10 kHz, respectively. The temporal resolution and radial spatial resolution are 1 minute and 30 m, respectively. During the experiment, the lidar operates in the velocity azimuth display (VAD) scanning mode with an elevation angle of 70°. The key parameters of the CDWL are listed in Table 1.

The local meteorological data are provided by the MinFeng County Meteorological Bureau, including air temperature, ground temperature, relative humidity, horizontal visibility, etc.

ERA5 (Hersbach et al., 2020) is the fifth-generation global climate reanalysis dataset from the European Centre for Medium-Range Weather Forecasts (ECMWF). In this paper, ERA5 reanalysis data, such as μ-v-ω wind vector, atmospheric temperature, relative humidity, mean sea level pressure, surface latent heat flux, boundary layer height, etc. are applied to analyze the

https://doi.org/10.5194/egusphere-2024-1010
Preprint. Discussion started: 15 May 2024

regional variation of the whole desert. The spatial resolution of the reanalysis data is 0.25°×0.25°, and the temporal resolution is 1 hour.

Table 1. Key Parameters of the CDWL

Parameter	Value
Wavelength	1.5 μm
Pulse energy	130 μJ
Pulse repletion frequency	10 kHz
Diameter of telescope	100 mm
Radial spatial resolution	30 m
Azimuth scanning range	0-360°
Zenith angle	70°
Sample rate of ADC	500 MS/s

2.3 Methods

The data of CDWL has the characteristics of high radial spatial and temporal resolution, and can be used to estimate turbulent kinetic energy dissipation rate (TKEDR) at different heights. The backscatter signal and turbulence intensity detected by CDWL are sharply reduced due to the temperature inversion characteristic of the atmospheric boundary layer top (Hooper and Eloranta, 1986). Based on this, the TKEDR threshold method combined with the range-corrected carrier-to-noise ratio (CNR) wavelet transform method can effectively estimate the height of ABL (Smalikho and Banakh, 2017; Banakh et al., 2017; Banakh et al., 2021; Wang et al., 2021). A threshold of 10^{-4} m^2 s^{-3} is applied here. The covariance transform of the function (Brooks, 2003) is defined as:

$$W(a,b) = \frac{1}{a}\int_{R_b}^{R_t} X(R)h(\frac{R-b}{a})dR \quad (1)$$

where R is height. b is the smooth center position of the function. a is the dilation factor of the function, which is generally an integer multiple of the radial spatial resolution, and the value of 250 m was used in this paper. R_t and R_b represent the top and bottom heights of the range-corrected CNR, respectively. The Haar function is defined as:

$$h\left(\frac{R-b}{a}\right) = \begin{cases} -1, & b-\frac{a}{2} \le R \le b \\ 1, & b \le R \le b+\frac{a}{2} \\ 0, & others \end{cases} \quad (2)$$

The same type of CDWL also realizes the calculation and verification of TKEDR and BLH in various application scenarios (Wang et al., 2021; Wang et al., 2022; Jiang et al., 2022; Yuan et al., 2020; Yuan et al., 2021; Wu et al., 2023; Li et al., 2023).

https://doi.org/10.5194/egusphere-2024-1010
Preprint. Discussion started: 15 May 2024

3 Lidar results and local analysis

The underlying surface of the desert makes the night temperature drop greatly, so that the inversion layer (IL) is more likely to be formed at night. Compared with the night, the change of the mixed boundary layer height during the daytime can better reflect the development of local dust pollution. In this paper, the probability of monthly occurrence of boundary layer at different heights during the daytime (8:00 LT~21:00 LT) from September 2021 to August 2022 has collected the statistics, and the number of samples is 50663. It can be clearly seen from the Figure 2 that a small number of boundary layer heights developed more than 5 km on June 2022. In order to explain this phenomenon, the typical boundary layer data on 6 June, 2022 were selected for analysis.

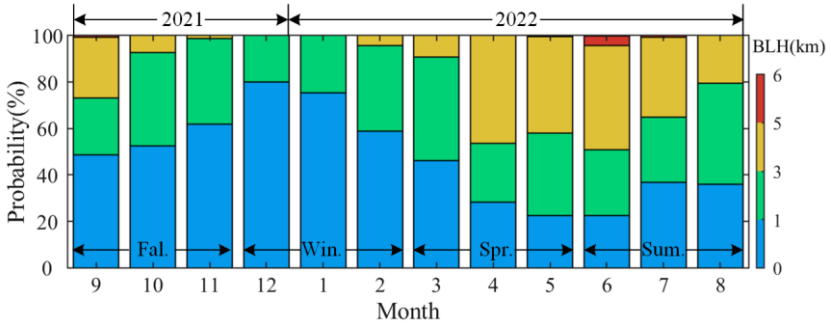

Figure 2. The monthly probability distribution of the boundary layer height of MinFeng in the Taklimakan Desert during the daytime from September 2021 to August 2022.

Fig. 3 shows the continuous observation results of the CDWL, the local meteorological equipment, and the ERA5 on 6 June, 2022, local time (UTC+8). The radial spatial resolution of the CDWL is 30 m. By analyzing the original data of power spectrum, the data such as CNR, TKEDR, vertical wind speed, horizontal wind speed and horizontal wind direction were obtained. The CNR or backscattering coefficient can be used as an indicator of aerosol concentration (Pea et al., 2013). When the CNR value is less than -17 dB, the calculated product value is regarded as an invalid value. In this paper, 0:00 LT~12:00 LT is divided into the low-level jet (LLJ) stage, and 12:00 LT~24:00 LT is divided into the thermal effect stage.

The LLJ generally refers to the strong and narrow airflow zone with wind speed greater than 12 m s^{-1} within 3 km height (Bonner, 1968). It can be seen from Fig. 3b that there is an obvious LLJ phenomenon in the study area before 12:00 LT, and the central axis of the LLJ is located at about 1 km.

At 0:00 LT~6:00 LT, before the formation of the LLJ, the downhill airflow blowing from the TP to the desert was superimposed on the desert background wind field. As shown in Fig. 3(a-b), the horizontal wind speed was increased to a maximum of 16.62 m s^{-1} at 5:41 LT, which reached a critical sand-raising wind speed of 3.5~10.9 m s^{-1} (Yang et al., 2017) and promoted the formation of LLJ (Matsumoto and Ninomiya, 1971; Mcnider and Pielke, 1981). The turbulence activity near the surface was also enhanced, and the BLH was stabilized at about 1 km (Fig. 3c). In addition, according to the local meteorological data, the study site had dust weather during this period (Fig. A1).

https://doi.org/10.5194/egusphere-2024-1010
Preprint. Discussion started: 15 May 2024

At 6:00 LT~12:00 LT, this period is the maintenance stage of the LLJ. In Fig. 3(f-g), it can be found that during the period of 6:00 LT~10:00 LT, with the cold downhill airflow traveled to the desert basin, the near-surface temperature dropped sharply and the relative humidity increased significantly. Meanwhile, the surface weather station also recorded that the difference of the ground-air temperature reached a minimum of -0.8 °C at 8:00 LT. At 6:00 LT~8:00 LT, firstly, as shown in Fig. 3a, the downward transfer of momentum may have caused the dust aerosol to lift into the residual layer at about 3 km (Washington et al., 2006; Fiedler et al., 2013), and promoted the dust aerosol in the residual layer to be supplemented from the desert hinterland. Secondly, due to the height of the inversion layer in the meteorology also often refers to the height of the ABL, so it can be seen from Fig. 3c that the downhill cold airflow weakened the intensity of the IL, reduced the height of the IL, and formed a near-surface IL (also analyzed in Fig. 5(p-t)). At 7:58 LT, the maximum wind speed of 15.04 m s^{-1} was reached, and the strong wind shear effect beneath the LLJ can provide a momentum source for turbulent activity and cause intermittent pulsation of turbulence (Ohya et al., 2006; Mathieu et al., 2005), so that the BLH can be raised to more than 2 km and the material in the residual layer may be partially supplemented.

The LLJ and IL can provide sufficient momentum, energy and material preparations for the development of the deep CBL during the period from 8:00 LT to 11:00 LT. Firstly, it can be seen from Fig. 3(a-b), due to the existence of the LLJ and the IL, the atmosphere formed a stratification state (Blackadar, 1957), so that the high concentration of CNR values were distributed below 1 km, which can provide a material basis for the development of the boundary layer. Secondly, the LLJ and the IL can play a role in maintaining the balance of atmospheric thermal structure, inhibiting the internal turbulent motion and energy exchange with the upper atmosphere, and storing enough momentum and energy for the development of deep CBL. Finally, the weakening of the height and stability of the IL enables the developing boundary layer to reduce the energy of the broken IL, which is conducive to the vigorous development of the subsequent boundary layer.

At 12:00 LT~19:00 LT, with the shortwave radiation of the sun gradually heating the atmosphere and the driving force provided by the LLJ, the stable stratification at low altitude was broken, and the turbulent mixing process began to be reactivated. In Fig.3 (c-d), it can be seen that the values of TKEDR were always maintained in a large range and the vertical transport capacity of the atmosphere was enhanced significantly (Wang et al., 2020). Therefore, it can be found that the underlying CNR value below 1 km in Fig. 3a increased greatly, and the height of the CBL in Fig. 3c was rapidly developed and exceeded 5 km (Meng et al., 2019). Due to the existence of the LLJ and the IL in the early stage, the dust aerosol was distributed below 1 km. The lower dust aerosol layer can quickly absorb solar radiation and heat the atmosphere, which can form a “furnace effect” (Ma et al., 2021; Ma et al., 2020) to make the material conditions of the desert boundary layer develop rapidly into thermal conditions. It can be seen from Fig. 3a and Fig. 3c that the temperature difference of ground-air reached a maximum of 25 °C at 15:00 LT, the height of the CBL is increasing rapidly at about 13:00 LT. This strong thermal effect rapidly promoted the growth of the CBL. The LLJ with large wind speed can also provide a basic dynamic condition for the development of the CBL, and the lifting process of the horizontal wind can be obviously found at 12:00 LT in Fig. 3b. The TP has the characteristics of high altitude, thin air, and little weakening effect on solar radiation, so that the sensible heat heating of the surface of TP can suck up the surrounding atmosphere and form a “sensible heat driven air-pump” of the TP (TP-SHAP) (Wu et al., 2012; Wu et al.,

https://doi.org/10.5194/egusphere-2024-1010
Preprint. Discussion started: 15 May 2024

2007). The study site of this paper is located in the northern foot of the TP, and the TP-SHAP has a strong effect of lifting dust aerosols (Tan et al., 2021), which can lift dust aerosols from the bottom of the desert along the northern slope of the Kunlun Mountains to the TP (Ge et al., 2014), thus further promoting the development of the local boundary layer (analyzed in Fig. 7). Finally, the role of continuous hot weather and the entrainment process of the residual layer cannot be ignored (Zhang et al., 2011; Marsham et al., 2008). The local meteorological data show that the hot weather greater than 30 °C has lasted for 6 days.

At 17:00 LT~24:00 LT, the study site began to be covered by clouds. The presence of clouds can greatly weaken the solar radiation reaching the surface and make the surface temperature decrease rapidly. At 17:00 LT~20:00 LT, due to the surface temperature is still much higher than the atmospheric temperature, and the heat preservation effect of dust on the atmosphere can continue to provide energy for the upper atmosphere, so the atmospheric turbulence is still maintained in an active state. After the surface radiation further cooled the near-surface air, the ground-air temperature difference changed to -0.6 °C at 22:00 LT. After the boundary layer developed into a nocturnal stable boundary layer (SBL), the airflow began to recover into a relatively strong and narrow airflow zone (Hoecker, 1963).

The local surface meteorological observation data of the day are shown in Fig. A1. At the experimental site, the representative CNR, horizontal wind speed, TKEDR, BLH, vertical wind speed and wind direction in different seasons are also shown in Fig. A2.

https://doi.org/10.5194/egusphere-2024-1010
Preprint. Discussion started: 15 May 2024

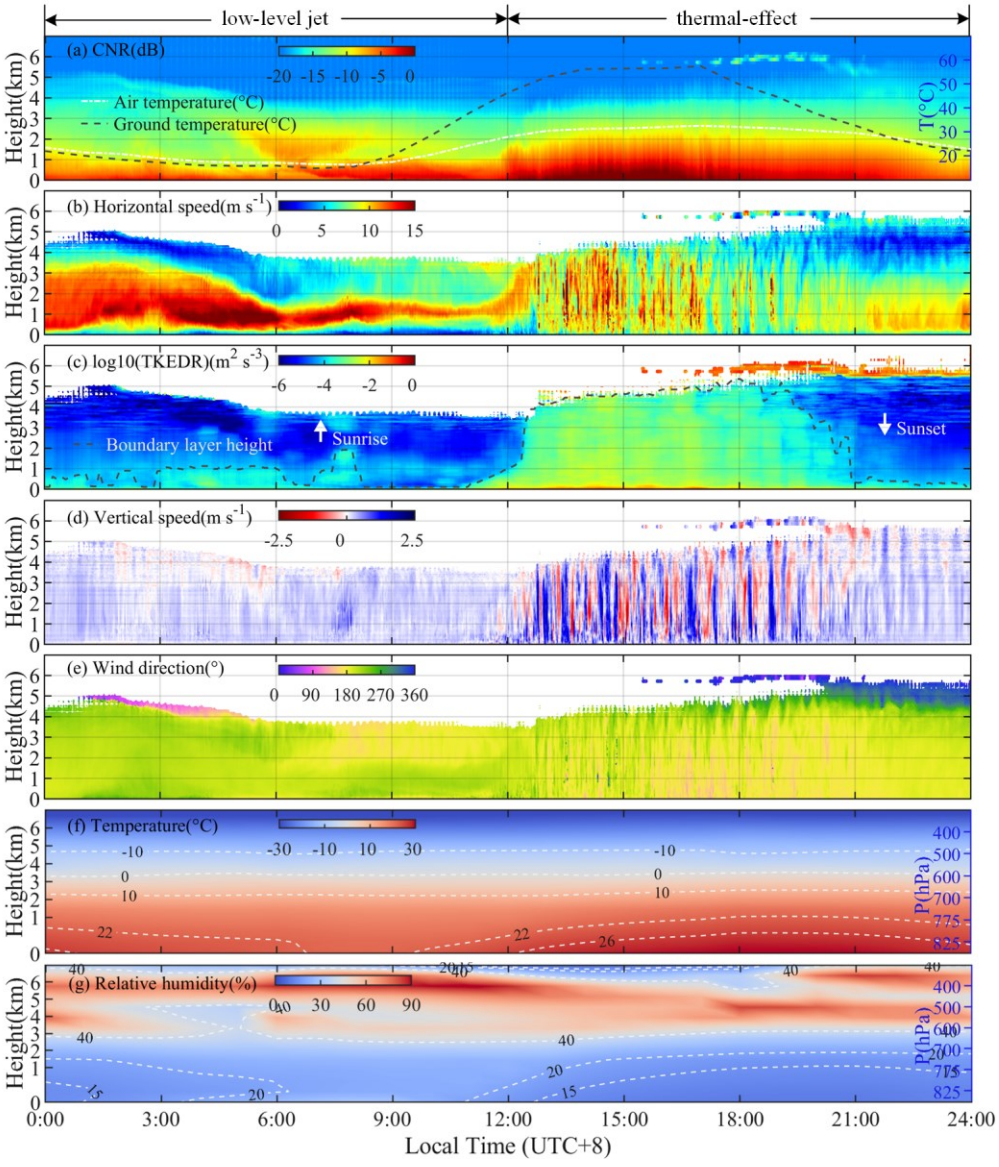

Figure 3. The continuous observation results of the CDWL, the local meteorological equipment, and the ERA5 on 6 June, 2022, local time (UTC+8). (a) CNR, the local air and ground temperatures are also shown in this subgraph. (b) horizontal wind speed. (c) log10(TKEDR) and boundary layer height, the time of sunrise and sunset are marked with arrow symbols. (d) vertical wind speed, the positive vertical wind speed represents the descending speed, and vice versa. (e) horizontal wind direction, 0° represents the wind blows to the north. (f) atmospheric temperature. (g) relative humidity. The height represents the height above the ground of the lidar site. The temperature and relative humidity contours in Fig. 3f and Fig. 3g are denoted by white dashed lines.

https://doi.org/10.5194/egusphere-2024-1010
Preprint. Discussion started: 15 May 2024

4 ERA5 results and regional analysis

4.1 Low-level jet

The LLJ is closely related to air pollution, dust storm, heavy rainfall and many other aspects. Studying the LLJ can partially reveal the dust emission and transmission process in the study area. Fig. 4 shows the variations of wind vector, geopotential height, atmospheric temperature, and relative humidity of the TD at 750 hPa (about 1.05 km above the ground) from 2:00 LT to 10:00 LT. It can be seen from the wind vector subgraph of Fig. 4(a-e) that the study site is located in the LLJ region. In Fig. 4(a-c), the upstream and downstream of the horizontal airflow correspond to the divergence region (with lower temperature and relative humidity) and the convergence region (with higher temperature and relative humidity), respectively. The horizontal airflow can make the divergence of the upstream region sink and the convergence of the downstream region rise, which is conducive to the development of the subsequent LLJ and the transport of dust aerosols (Bonner, 1968; Han et al., 2022). The TD is surrounded by three mountains, forming a unique horseshoe-shaped terrain structure. At the northeast of the study site, the northwest wind with lower wind speed deflects to the west after encountering the blocking of the TP. In order to ensure the conservation of the potential vorticity, the east wind with higher wind speed is formed. The blocking of the mountains further catalyzes the formation of the LLJ (Wexler, 1961) and may also play a role in the transport of dust aerosols (Caton Harrison et al., 2021). Compared with the northern side of the desert, the southern side has higher temperature, lower geopotential height and relative humidity, which is conducive to the formation of more active airflow. Under the background conditions of thermal and potential difference, it is helpful to the formation and enhancement of the desert background wind field such as gradient wind and thermal wind, and to promote the formation of LLJ (Stensrud, 1996; Rife et al., 2010). At night in the TD, the wind field of the LLJ rotates clockwise and has a typical inertial oscillation phenomenon (Blackadar, 1957).

https://doi.org/10.5194/egusphere-2024-1010
Preprint. Discussion started: 15 May 2024

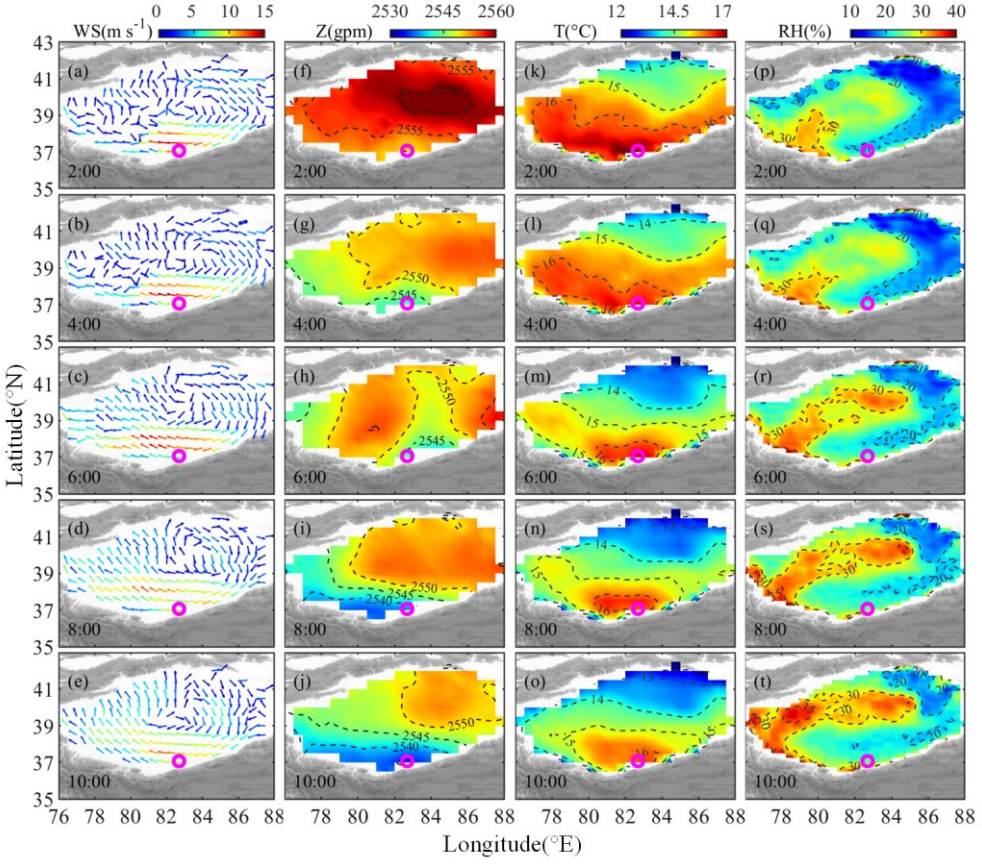

Figure 4. The distributions of ERA5 data over the Taklimakan Desert at 750 hPa (about 1.05 km above the ground) from 2:00 LT to 10:00 LT, on 6 June, 2022, local time (UTC+8). (a-e) wind vector. (f-j) geopotential height. (k-o) air temperature. (p-t) relative humidity. The purple circle represents the study site of MinFeng. The contours are denoted by dashed lines.

Fig. 5 shows the distribution of mean sea level pressure, surface sensible heat flux, surface latent heat flux, temperature inversion distribution, and BLH. At 2:00 LT~8:00 LT, it can be found that the pressure of the TP (1025 hPa) is much higher than that near the study site in the desert basin (1007 hPa) from Fig. 5(a-d). Therefore, a large pressure gradient was formed between the TP and the TD, which can promote the formation of the downhill airflow under the combined action of gravity and pressure gradient force. When the airflow of the downhill is superimposed on the background wind field of the TD, the wind speed of the TD can be enhanced (similar to Fig. 3b), which also indicates that the influence of topographic baroclinicity is significant (Jones, 2019). During this period, the surface sensible heat flux at the study site is generally greater than -10 W m^{-2}, and the surface latent heat flux is positive. The distribution of these fluxes will inhibit the convection and turbulence activities in the boundary layer, which is beneficial to the development of the nocturnal SBL (Zhang et al., 2017). At the study site, the most obvious IL phenomenon was formed at 8:00 LT. The boundary layer height of the study site was also located in the bigger value area of the whole desert (0.25 km contour line).

https://doi.org/10.5194/egusphere-2024-1010
Preprint. Discussion started: 15 May 2024

At 8:00 LT~10:00 LT, with the increase of solar radiation, the average sea level pressure on the southeast TP gradually decreased, the inversion layer began to dissipate, and the sensible and latent heat fluxes of the desert increased rapidly.

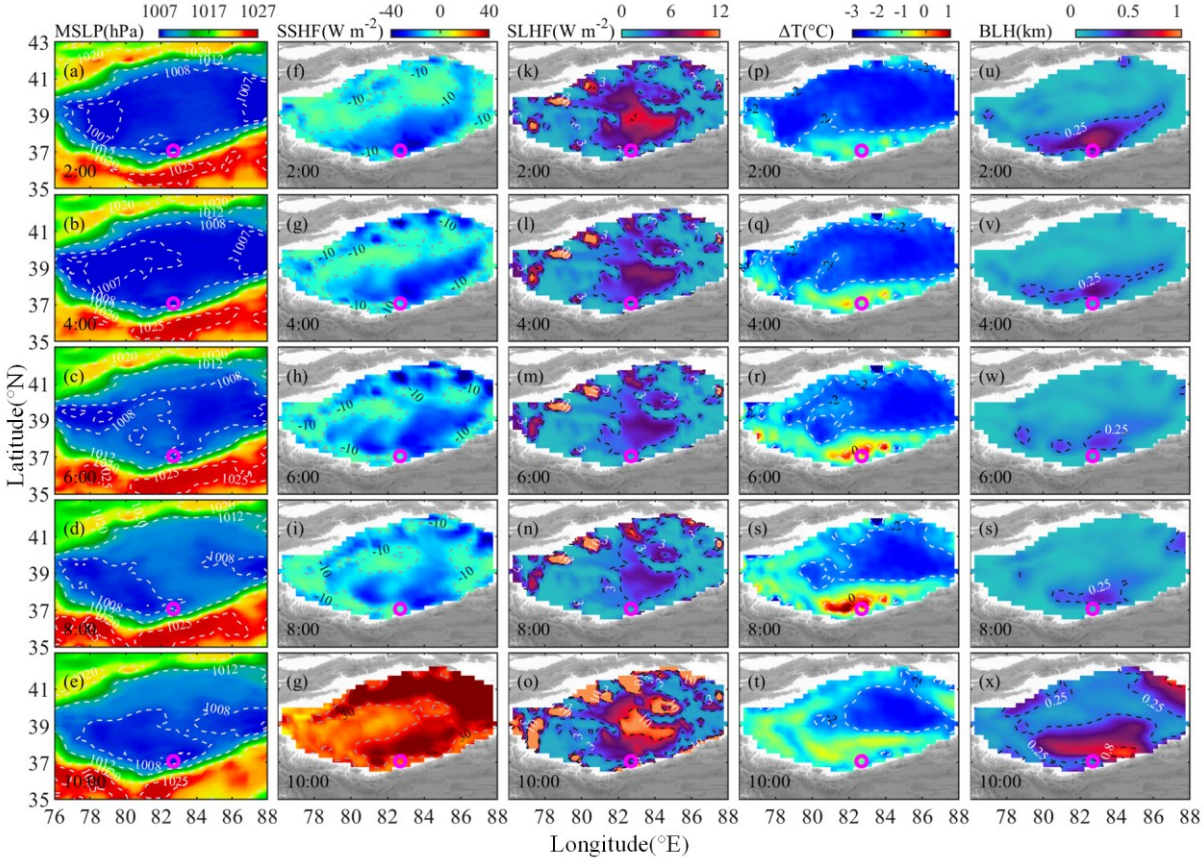

Figure 5. The distributions of ERA5 data over the Taklimakan Desert from 2:00 LT to 10:00 LT, on 6 June, 2022, local time (UTC+8). (a-e) mean sea level pressure. (f-j) surface sensible heat flux. (k-o) surface latent heat flux. (p-t) temperature inversion distribution, obtained by subtracting 850 hPa (38 m above the ground) from the temperature data of 825 hPa (232 m above the ground). (u-x) boundary layer height. The purple circle represents the study site of MinFeng. The contours are denoted by dashed lines.

4.2 Heat factors

In June, the precipitation in the study region is scarce, the underlying surface is dominated by fine sand, and the soil is dry with strong evaporation capacity. Fig. 6 shows the distribution of wind vector, air temperature, surface sensible heat flux, surface latent heat flux and boundary layer height over the TD from 12:00 LT to 22:00 LT. At 12:00 LT~18:00 LT, with the dissipation of the LLJ, the study site gradually shifted from the east wind to the northeast wind blowing towards the TP. The continuous high solar radiation made the surface sensible heat flux near the study site greater than 300 W m^{-2} (at 16:00 LT), so the efficiency of heating the atmosphere will be very high (Zhang et al., 2002). Firstly, heating the atmosphere with such a high surface sensible heat flux can promote the generation of thermal convection, thus strengthening the atmospheric

https://doi.org/10.5194/egusphere-2024-1010
Preprint. Discussion started: 15 May 2024

turbulence and making the boundary layer develop rapidly. Secondly, the atmospheric temperature of the study region is also always located in the relative highest value region at each moment (30 °C contour), so that the region can form a lower low-pressure center to gather dust from the relatively cold area. Therefore, at 18:00 LT, a deep CBL with a maximum of 4546 m was formed near the study site. At 20:00 LT~22:00 LT, the surface sensible heat flux turned to a negative value rapidly and the BLH decreased to less than 1 km.

Compared with the CDWL data, the temporal and spatial resolution of the ERA5 reanalysis data is more rough, and the calculation method of the BLH is also different, resulting in the inversion of the maximum height of deep CBL lower than the CDWL.

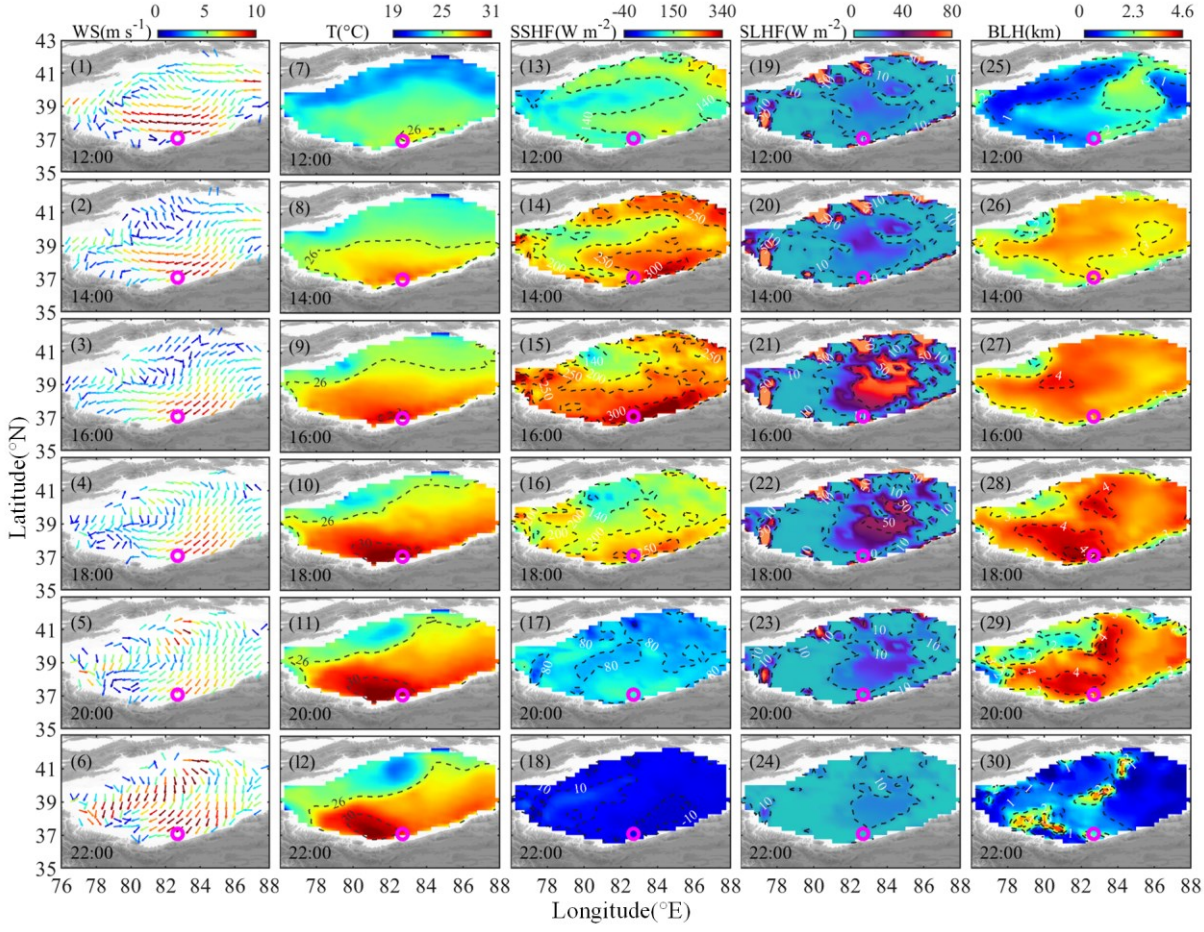

Figure 6. The distributions of ERA5 data over the Taklimakan Desert from 2:00 LT to 10:00 LT, on 6 June, 2022, local time (UTC+8). (1-6) wind vectors (850 hPa, 38 m above the ground). (7-12) air temperature (850 hPa, 38 m above the ground). (13-18) surface sensible heat flux. (19-24) surface latent heat flux. (25-30) boundary layer height. The purple circle represents the study site of MinFeng. The contours are denoted by dashed lines.

Fig. 7 shows the variation of meteorological data in the vertical section of the TD at the nearest study site of MinFeng. In Fig. 7(a-e), the wind vector is synthesized by v and scaled ω (ω scaled by 10), which is used to observe the atmospheric vertical

https://doi.org/10.5194/egusphere-2024-1010
Preprint. Discussion started: 15 May 2024

motion of the TD. The elevation of the study site MinFeng is 1418 m. The Richardson number (Ri) can reflect the influence of vertical shear of horizontal wind on atmospheric stability and the state of atmospheric turbulence (Stull, 1988). There is a certain deviation in selecting different Ri values to identify the BLH (Guo et al., 2016). Generally, the value of Ri less than or equal to 0.25 is used to represent the turbulent motion state of the atmosphere, and the value of 0.25 is used to identify the BLH (Zhang et al., 2013). At 12:00 LT, the near-surface potential temperature on the left side is higher than that on the right side, and the 20 % relative humidity and the Ri critical value 0.25 contour line are maintained at a lower elevation.

At 14:00 LT~18:00 LT. In the elevation range of 1.4 km to 5 km, firstly, the potential temperature on the north side of the TP is almost constant with elevation (Fig. 7(h-i), 316K), indicating that the rate of temperature reduction during the rapid heating and expansion of the air is greater than the rate of dry adiabatic cooling, forming an atmospheric superadiabatic expansion process. In this atmospheric state, a strong updraft can be formed (Fig. 7(b-c)), which makes the atmosphere in an unstable state. The obvious uplift process can be seen in the 0.25 Ri contour in Fig. 7(q-s) and the 20% relative humidity contour in Fig. 7(l-n). This atmospheric superadiabatic expansion process is very conducive to the diffusion and transport of dust aerosols and the development of boundary layer (Arnette et al., 1998; Nilsson et al., 2001). This phenomenon also provides evidence that TKEDR is maintained within a large numerical range in Fig. 3c. Secondly, the topography and potential temperature of the south side of the desert basin are higher than that of the north side, forming an airflow from the northern side to the southern side (Fig. 7(b-c)), so that the dust aerosol can climb and transport along the Kunlun Mountains to the TP. Above the elevation of 5 km, the higher potential temperature area is distributed in the left TP, which can form the TP-SHAP. Firstly, the gradient of the potential temperature of the TP is much higher than that of the desert basin, which makes the atmosphere unstable and easier to form atmospheric convective motion, and vertically suck dust aerosols around the TP (Jia et al., 2015; Wu et al., 2017; Feng et al., 2020). Secondly, at the same height, the potential temperature on the left side is higher than that on the right side, and the potential temperature slope on the left side is also larger, which can form a horizontal suction of dust aerosols over the desert.

At 20:00 LT, the cold air invaded the TD (Fig. 3a and Fig. 7o) and intersected with the warm air over the desert to form a cold front, and the cold air sank (Fig. 7j) to force the desert basin to produce a strong upward motion (Fig. 7e).

https://doi.org/10.5194/egusphere-2024-1010
Preprint. Discussion started: 15 May 2024

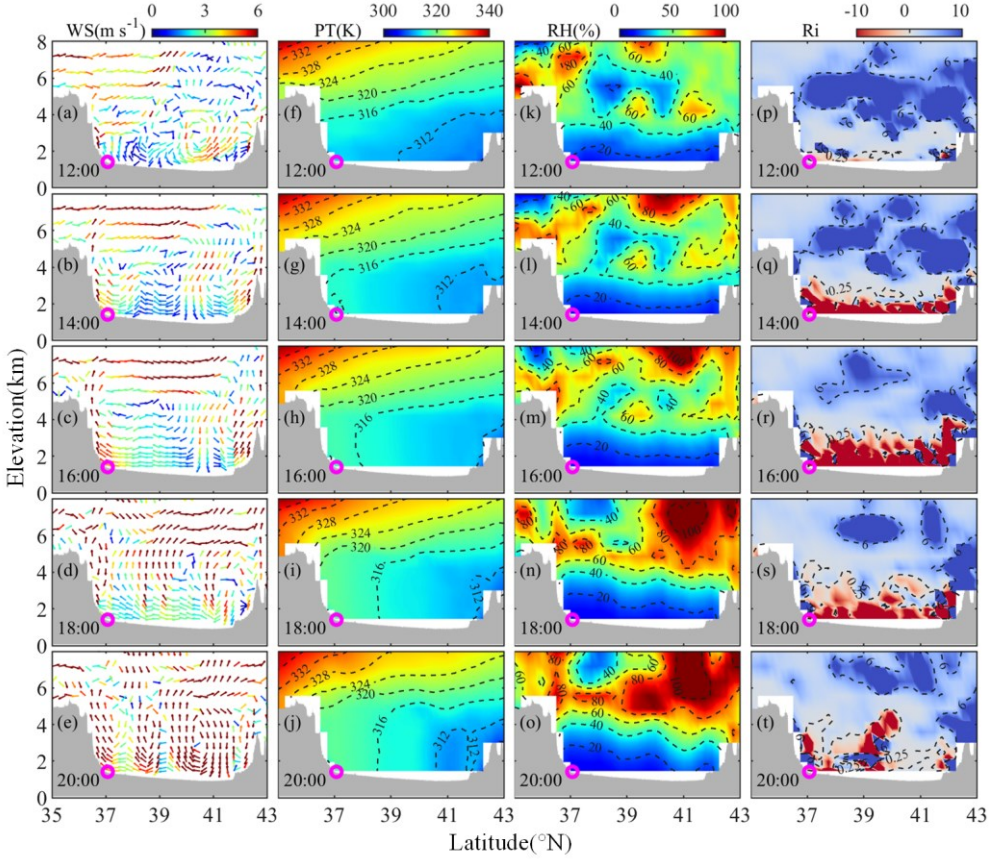

Figure 7. The meteorological elements in the vertical section of the Taklimakan Desert at the study site from 12:00 LT to 20:00 LT, on 6 June, 2022, local time (UTC+8). (a-e) wind vectors (synthesized by v and scaled ω, ω scaled by 10). (f-g) potential temperature. (k-o) relative humidity. (p-t) Richardson number. The purple circle represents the study site of MinFeng. The leftmost of the study site is the Tibet Plateau.

5 Conclusion

In this study, the CDWL data and ERA5 reanalysis data were used to comprehensively analyze the development process of a representative deep convective boundary layer on the southern edge of the Taklimakan Desert and the northern foot of the Tibet Platea on 6 June, 2022. The special geographical location of the study site makes the formation of deep convective boundary layer more complicated. The results show that the low-level jet and temperature inversion layer have made sufficient momentum, energy and material preparations for the development of the atmospheric boundary layer, and the thermal effect promoted the formation of a deep convective boundary layer. The schematic diagram of the development of the low-level jet and the deep convective boundary layer is shown in Fig. 8.

https://doi.org/10.5194/egusphere-2024-1010
Preprint. Discussion started: 15 May 2024

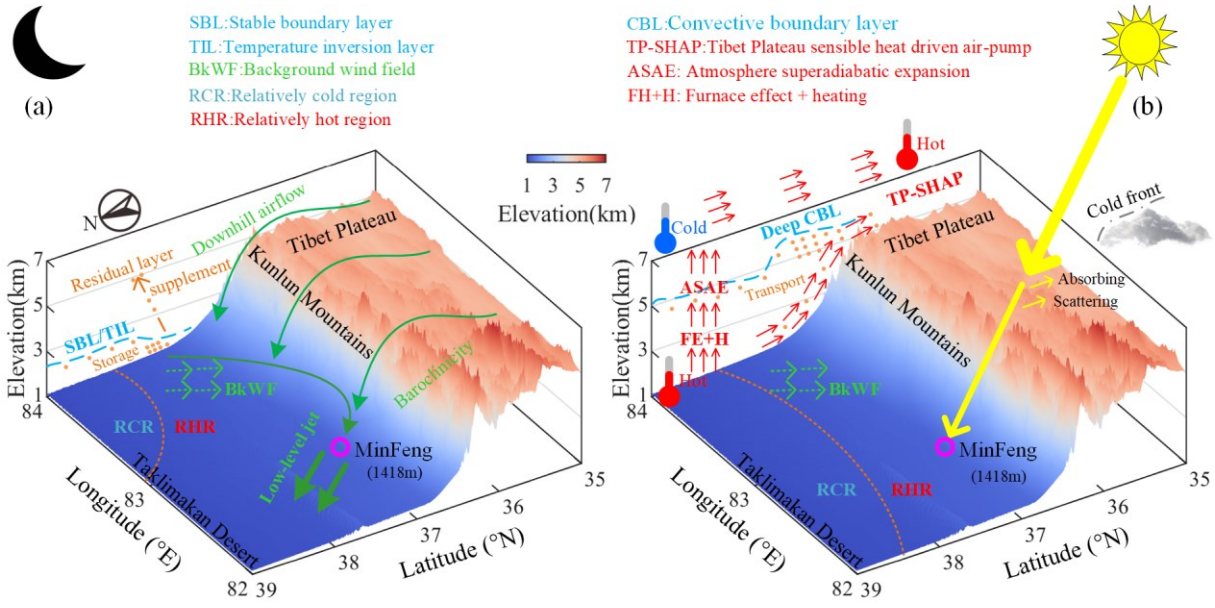

Figure 8. A schematic diagram of the development of low-level jet and deep convective boundary layer. (a) before sunrise. (b) before sunset.

The formation of low-level jet in the study site is the combined effect of multiple factors. The first is the pressure gradient force and thermal difference between the north and south of the desert, which can form a background wind field from north to south. Secondly, the terrain blocking effect of the Tibet Plateau makes the northwest wind with lower wind speed deflect into the east wind with higher wind speed. Then the terrain baroclinicity of the Tibet Plateau is easy to form downhill airflow at night, and when the downhill airflow is superimposed on the background wind field, the wind speed of the background wind field will be enhanced. Finally, the divergence structure of the upstream airflow and the convergence structure of the downstream airflow promote the development of the low-level jet.

The low-level jet and the inversion layer also play an important role in the development of the deep convective boundary layer. Firstly, the cold downhill wind is one of the factors of the formation of the low-level jet, which can weaken the height and strength of the inversion layer, thus reducing the energy demand of the broken inversion layer. Secondly, the low-level jet can not only cause intermittent turbulence pulsation, but also inhibit the exchange of energy and material with the lower atmosphere, so as to provide key material and energy supplement for the development of the deep convective boundary layer. Then, the low-level jet can provide a dynamic basis for the subsequent development of the boundary layer. Finally, the existence of the inversion layer and the low-level jet can inhibit the internal turbulent motion in the lower atmosphere, and make the dust aerosol accumulate near the ground, thus providing material basis and storing sufficient momentum and energy for the subsequent development of the deep convective boundary layer.

The underlying surface of the desert itself has a strong heating effect on the atmosphere, and the corresponding thermal factors can catalyze the formation of the deep convective boundary layer. First of all, the accumulation of dust aerosols at low altitude in the desert can form a furnace effect, so that the material conditions for the development of the desert atmosphere boundary

https://doi.org/10.5194/egusphere-2024-1010
Preprint. Discussion started: 15 May 2024

layer can be quickly transformed into thermal conditions, and promote the formation of the atmospheric superadiabatic expansion process. Secondly, the thermal effect of the Tibet Plateau sensible heat driven air-pump can suck up the atmosphere around the plateau and lift dust aerosols. Finally, the cold front transit can produce strong convective motion in the desert area. Overall, the results reveal the formation process of a typical deep convective boundary layer in the Taklimakan Desert, and also reflect the process of land-atmosphere momentum, energy and material exchange and transport between the Taklimakan Desert and the Tibetan Plateau. However, the data range of CDWL only contains a point area of MinFeng, and lacks the observation results of the mountains along the northern side of the Tibet Plateau. The follow-up work will be combined with multi-site observations of Raman lidar and weather radar to study the transmission characteristics of dust to the Tibet Plateau, as well as the long-term statistical analysis of the effects of extreme weather such as drought and dust storm on the boundary layer height.

Data availability

The ERA5 data sets are publicly available from ECMWF website at https://cds.climate.copernicus.eu. The two datasets used in ERA5 are "ERA5 hourly data on pressure levels from 1940 to present" and "ERA5 hourly data on single levels from 1940 to present". The CDWL datas can be downloaded from https://figshare.com/articles/dataset/deep_CBL_lidar_datas/25434556 (Su et al., 2024).

Appendix A: Local observational and CDWL results during the experiment

The surface meteorological observation data on 6 June, 2022 (UTC + 8) are shown in Fig. A1. The CNR, horizontal wind speed, log10(TKEDR) and boundary layer height, vertical wind speed, wind direction during the field experiment in different seasons are shown in Fig. A2.

https://doi.org/10.5194/egusphere-2024-1010
Preprint. Discussion started: 15 May 2024

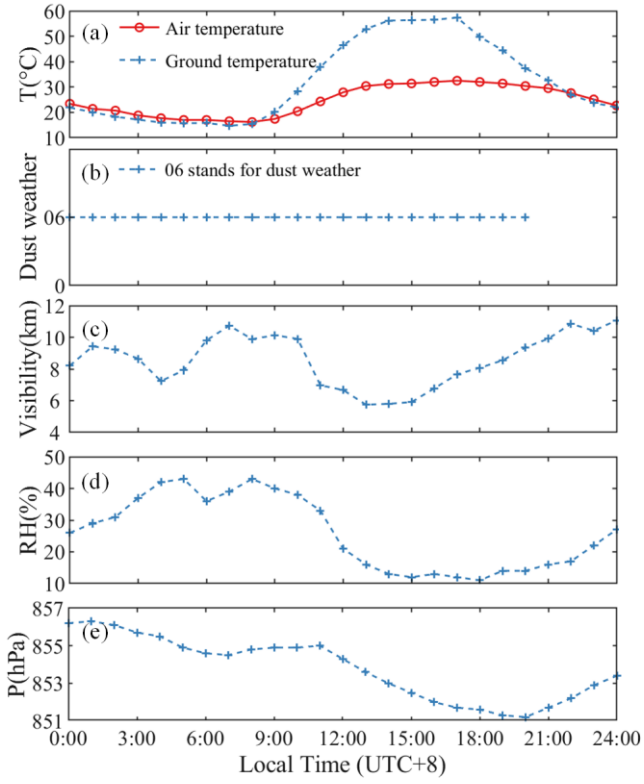

Figure A1. The surface meteorological observation data on 6 June, 2022, (UTC+8). (a) temperature. (b) dust weather. (c) horizontal visibility. (d) relative humidity. (e) local atmospheric pressure.

https://doi.org/10.5194/egusphere-2024-1010
Preprint. Discussion started: 15 May 2024

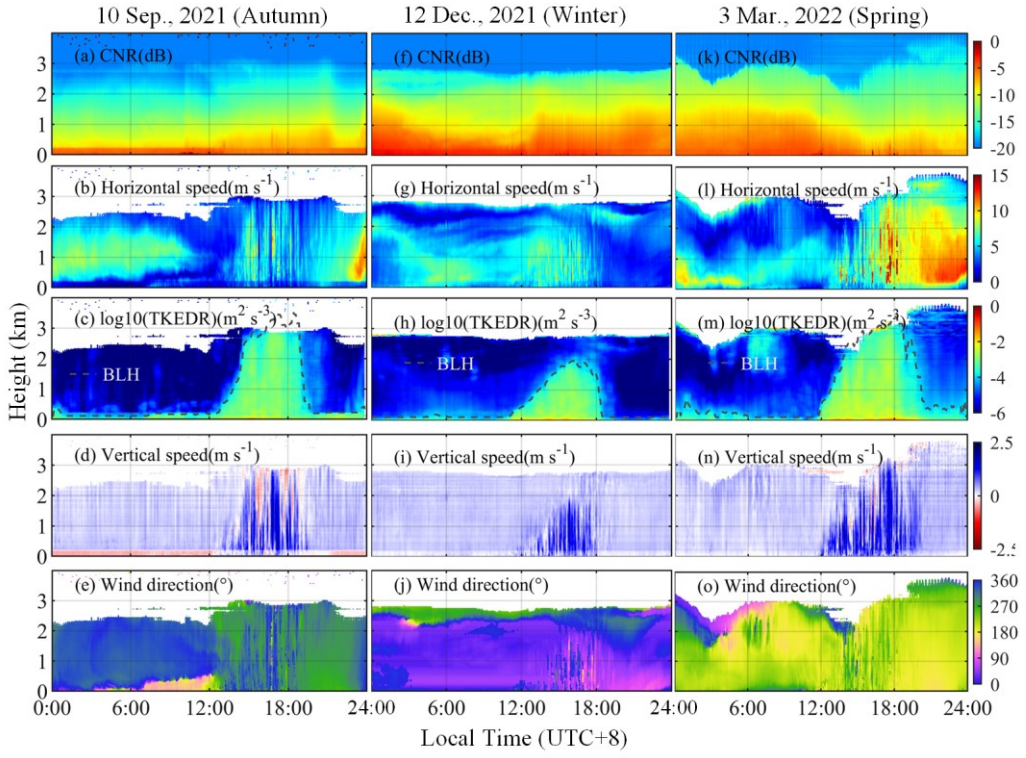

Figure A2. The continuous observation results of CDWL in different seasons. (a-e) 10 Sep., 2021. (f-j) 12 Dec., 2021. (k-o) 3 Mar., 2022.

Author contribution

HX conceived, designed the study. LS and JY performed the lidar experiments. LS performed the analysis of lidar data and ERA5 data. XW and QH provide the field experiment site and the local meteorological data. LS carried out the analysis and prepared the figures, with comments from other co-authors. LS, LC and JY wrote the manuscript. All authors read and approved the final manuscript.

Competing interests.

The authors declare that they have no conflict of interest.

https://doi.org/10.5194/egusphere-2024-1010
Preprint. Discussion started: 15 May 2024

Acknowledgements.

Thanks for the support of the Xinjiang Uygur Autonomous Region Meteorological Service and the Desert Meteorological Institute of China Meteorological Administration for this experiment and local meteorological data; The European Centre for Medium-Range Weather Forecasts for providing support with atmospheric reanalysis data.

References

Arnette, S. A., Samimy, M., and Elliott, G. S.: The effects of expansion on the turbulence structure of compressible boundary layers, Journal of Fluid Mechanics, 367, 67-105, 10.1017/S0022112098001475, 1998.

Banakh, V., Smalikho, I., and Falits, A.: Estimation of the turbulence energy dissipation rate in the atmospheric boundary layer from measurements of the radial wind velocity by micropulse coherent Doppler lidar, Optics Express, 25, 22679-22692, 10.1364/OE.25.022679, 2017.

Banakh, V. A., Smalikho, I. N., and Falits, A. V.: Estimation of the height of the turbulent mixing layer from data of Doppler lidar measurements using conical scanning by a probe beam, Atmospheric Measurement Techniques, 14, 1511-1524, 10.5194/amt-14-1511-2021, 2021.

Basha, G. and Ratnam, M. V.: Identification of atmospheric boundary layer height over a tropical station using high-resolution radiosonde refractivity profiles: Comparison with GPS radio occultation measurements, Journal of Geophysical Research, 114, D16101, 10.1029/2008JD011692, 2009.

Birch, C. E., Parker, D. J., Marsham, J. H., and Devine, G.: The effect of orography and surface albedo on stratification in the summertime Saharan boundary layer: Dynamics and implications for dust transport, Journal of Geophysical Research, 117, 10.1029/2011JD015965., 2012.

Blackadar, A. K.: Boundary Layer Wind Maxima and Their Significance for the Growth of Nocturnal Inversions, Bulletin of the American Meteorological Society, 38, 283-290, 10.1175/1520-0477-38.5.283, 1957.

Bonner, W. D.: Climatology of the low level jet, Monthly Weather Review, 96, 833-850, 10.1175/1520-0493(1968)096<0833:COTLLJ>2.0.CO;2, 1968.

Brooks, I. M.: Finding boundary layer top: Application of a wavelet covariance transform to lidar backscatter profiles, Journal of Atmospheric & Oceanic Technology, 20, 1092-1105, 10.1175/1520-0426(2003)020<1092:FBLTAO>2.0.CO;2, 2003.

Caton Harrison, T., Washington, R., Engelstaedter, S., Jones, R., and Savage, N. H.: Influence of Orography Upon Summertime Low-Level Jet Dust Emission in the Central and Western Sahara, Journal of Geophysical Research: Atmospheres, 126, 1-24, 10.1029/2021JD035025, 2021.

Che, J. and Zhao, P.: Characteristics of the summer atmospheric boundary layer height over the Tibetan Plateau and influential factors, Atmos Chem Phys, 21, 5253-5268, 10.5194/acp-21-5253-2021, 2021.

Collis, R.: Lidar: a new atmospheric probe, Quarterly Journal of the Royal Meteorological Society, 92, 220-230, 10.1002/qj.49709239205open, 1966.

https://doi.org/10.5194/egusphere-2024-1010
Preprint. Discussion started: 15 May 2024

Feng, X., Mao, R., Gong, D., Zhao, C., Wu, C., Zhao, C., Wu, G.-Q., Lin, Z., Liu, X., Wang, K., and Sun, Y.: Increased Dust Aerosols in the High Troposphere Over the Tibetan Plateau From 1990s to 2000s, Journal of Geophysical Research: Atmospheres, 125, 1-11, 10.1029/2020JD032807, 2020.

Fiedler, S., Schepanski, K., Heinold, B., Knippertz, P., and Tegen, I.: Climatology of nocturnal low-level jets over North Africa and implications for modeling mineral dust emission, Journal of Geophysical Research. Atmospheres, 118, 6100 - 6121, 10.1002/jgrd.50394, 2013.

Garratt, J. R.: The atmospheric boundary layer, Earth-Science Reviews, 37, 89-134, 10.1016/0012-8252(94)90026-4, 1994.

Ge, J., Huang, J., Xu, C., Qi, Y., and Liu, H.: Characteristics of Taklimakan dust emission and distribution: A satellite and reanalysis field perspective, Journal of Geophysical Research: Atmospheres, 119, 11,772-711,783, 10.1002/2014JD022280, 2014.

Guo, J., Miao, Y., Zhang, Y., Liu, H., Li, Z., Zhang, W., He, J., Lou, M., Yan, Y., Bian, L., and Zhai, P.: The climatology of planetary boundary layer height in China derived fromradiosonde and reanalysis data, Atmos Chem Phys, 16, 13309-13319, 10.5194/acp-16-13309-2016, 2016.

Han, B., Lü, S., and Ao, Y.: Development of the convective boundary layer capping with a thick neutral layer in Badanjilin: Observations and simulations, Advances in Atmospheric Sciences, 29, 177-192, 10.1007/s00376-011-0207-4, 2012.

Han, B., Zhao, C., Lü, S., and Wang, X.: A diagnostic analysis on the effect of the residual layer in convective boundary layer development near Mongolia using 20th century reanalysis data, Advances in Atmospheric Sciences, 32, 807-820, 10.1007/s00376-014-4164-6, 2015.

Han, Z., Ge, J., Chen, X., Hu, X., Yang, X., and Du, J.: Dust Activities Induced by Nocturnal Low-Level Jet Over the Taklimakan Desert From WRF-Chem Simulation, Journal of Geophysical Research: Atmospheres, 127, 10.1029/2021JD036114, 2022.

Hoecker, W. H.: Three southerly low-level jet systems delineated by the Weather Bureau special pibal network of 1961, Monthly Weather Review, 91, 573-582, 10.1175/1520-0493(1963)091<0573:TSLJSD>2.3.CO;2, 1963.

Holtslag, A. and Boville, B.: Local versus nonlocal boundary-layer diffusion in a global climate model, Journal of climate, 6, 1825-1842, 10.1175/1520-0442(1993)006<1825:LVNBLD>2.0.CO;2, 1993.

Hooper, W. P. and Eloranta, E. W.: Lidar Measurements of Wind in the Planetary Boundary-Layer - the Method, Accuracy and Results from Joint Measurements with Radiosonde and Kytoon, J Clim Appl Meteorol, 25, 990-1001, 10.1175/1520-0450(1986)025<0990:Lmowit>2.0.Co;2, 1986.

Jia, R., Liu, Y., Chen, B., Zhang, Z., and Huang, J.: Source and transportation of summer dust over the Tibetan Plateau, Atmospheric Environment, 123, 210-219, 10.1016/J.ATMOSENV.2015.10.038, 2015.

Jiang, P., Yuan, J., Wu, K., Wang, L., and Xia, H.: Turbulence detection in the atmospheric boundary layer using coherent Doppler wind lidar and microwave radiometer, Remote Sensing, 14, 2951, 10.5194/amt-2021-288, 2022.

Jones, C.: Recent changes in the South America low-level jet, npj Climate and Atmospheric Science, 2, 1-8, 10.1038/s41612-019-0077-5, 2019.

https://doi.org/10.5194/egusphere-2024-1010
Preprint. Discussion started: 15 May 2024

Lai, Y., Chen, X., Ma, Y., Sun, F., Zhou, D., and Xie, Z.: Variation of Atmospheric Boundary Layer Height Over the Northern, Central, and Southern Parts of the Tibetan Plateau During Three Monsoon Seasons, Journal of Geophysical Research: Atmospheres, 128, 1-14, 10.1029/2022JD038000, 2023.

Li, H., Yang, Y., Hu, X. M., Huang, Z., Wang, G., Zhang, B., and Zhang, T.: Evaluation of retrieval methods of daytime convective boundary layer height based on lidar data, Journal of Geophysical Research: Atmospheres, 122, 4578-4593, 10.1002/2016JD025620, 2017.

Li, M., Xia, H., Su, L., Han, H., Wang, X., and Yuan, J.: The Detection of Desert Aerosol Incorporating Coherent Doppler Wind Lidar and Rayleigh–Mie–Raman Lidar, Remote Sensing, 15, 5453, 10.3390/rs15235453, 2023.

Ma, Y., Xin, J., Wang, Z., Tian, Y., Wu, L., Tang, G., Zhang, W., de Arellano, J. V.-G., Zhao, D., Jia, D., Ren, Y., Gao, Z., Shen, P., Ye, J., and Martin, S. T.: How do aerosols above the residual layer affect the planetary boundary layer height?, The Science of the total environment, 151953, 10.1016/j.scitotenv.2021.151953, 2021.

Ma, Y., Ye, J., Xin, J., Zhang, W., Vilà-Guerau de Arellano, J., Wang, S., Zhao, D., Dai, L., Ma, Y., Wu, X., Xia, X. a., Tang, G., Wang, Y., Shen, P., Lei, Y., and Martin, S. T.: The Stove, Dome, and Umbrella Effects of Atmospheric Aerosol on the Development of the Planetary Boundary Layer in Hazy Regions, Geophysical Research Letters, 47, 1-10, 10.1029/2020GL087373, 2020.

Marsham, J. H., Parker, D. J., Grams, C. M., Grey, W. M. F., and Johnson, B. T. T.: Observations of mesoscale and boundary-layer circulations affecting dust uplift and transport in the Saharan boundary layer, Atmos Chem Phys, 8, 8817-8846, 10.5194/ACPD-8-8817-2008, 2008.

Mathieu, N., Strachan, I. B., Leclerc, M., Karipot, A., and Pattey, E.: Role of low-level jets and boundary-layer properties on the NBL budget technique, Agricultural and Forest Meteorology, 135, 35-43, 10.1016/j.agrformet.2005.10.001, 2005.

Matsumoto, S. and Ninomiya, K.: On the Mesoscale and Medium-scale Structure of a Cold Front and the Relevant Vertical Circulation, Journal of the Meteorological Society of Japan, 648-662, 1971.

McNider, R. T. and Pielke, R. A.: Diurnal Boundary-Layer Development over Sloping Terrain, Journal of the Atmospheric Sciences, 38, 2198-2212, 10.1175/1520-0469(1981)038<2198:DBLDOS>2.0.CO;2, 1981.

Meng, L., Yang, X.-h., Zhao, T., He, Q., Lu, H., Mamtimin, A., Huo, W., Yang, F., and Liu, C.: Modeling study on three-dimensional distribution of dust aerosols during a dust storm over the Tarim Basin, Northwest China, Atmospheric Research, 218, 285-295, 10.1016/J.ATMOSRES.2018.12.006, 2019.

Nilsson, E. D., Rannik, Ü., Kulmala, M., Buzorius, G., O'Dowd, C. D., and O'Dowd, C. D.: Effects of continental boundary layer evolution, convection, turbulence and entrainment, on aerosol formation, Tellus B: Chemical and Physical Meteorology, 53, 441 - 461, 10.3402/tellusb.v53i4.16617, 2001.

Ohya, Y., Nakamura, R., and Uchida, T.: Intermittent Bursting of Turbulence in a Stable Boundary Layer with Low-level Jet, Bound-Lay Meteorol, 126, 349-363, 10.1007/S10546-007-9245-Y, 2006.

Pea, Gryning, S.-E., Hahmann, and A., N.: Observations of the atmospheric boundary layer height under marine upstream flow conditions at a coastal site, Journal of Geophysical Research: Atmospheres, 118, 1924-1940, 10.1002/jgrd.50175, 2013.

https://doi.org/10.5194/egusphere-2024-1010
Preprint. Discussion started: 15 May 2024

Raman, S., Templeman, B., Templeman, S., Holt, T. R., Murthy, A., Singh, M. P., Agarwaal, P., Nigam, S., Prabhu, A., and Ameenullah, S.: Structure of the Indian southwesterly pre-monsoon and monsoon boundary layers: Observations and numerical simulation, Atmospheric Environment. Part A. General Topics, 24, 723-734, 10.1016/0960-1686(90)90273-P, 1990.

Rife, D. L., Pinto, J. O., Monaghan, A. J., Davis, C. A., and Hannan, J. R.: Global Distribution and Characteristics of Diurnally Varying Low-Level Jets, Journal of Climate, 23, 5041-5064, 10.1175/2010JCLI3514.1, 2010.

Smalikho, I. N. and Banakh, V. A.: Measurements of wind turbulence parameters by a conically scanning coherent Doppler lidar in the atmospheric boundary layer, Atmospheric Measurement Techniques, 10, 4191-4208, 10.5194/amt-10-4191-2017, 2017.

Stensrud, D. J.: Importance of Low-Level Jets to Climate: A Review, Journal of Climate, 9, 1698-1711, 10.1175/1520-0442(1996)009<1698:IOLLJT>2.0.CO;2, 1996.

Stull, R. B.: An Introduction to Boundary Layer Meteorology, Springer Science & Business Media, 10.1007/978-94-009-3027-8, 1988.

Su, L., Lu, C., Yuan, J., Wang, X., He, Q., and Xia, H.: Measurement report: The promotion of low-level jet and thermal-effect on development of deep convective boundary layer at the southern edge of the Taklimakan Desert, Figshare [dataset], 10.6084/m9.figshare.25434556.v1, 2024.

Tan, Z., Liu, Y., Zhu, Q., and Shao, T.: Impact of massive topography on the dust cycle surrounding the Tibetan Plateau, Atmospheric Environment, 264, 118703, 10.1016/J.ATMOSENV.2021.118703, 2021.

Wang, L., Yuan, J., Xia, H., Zhao, L., and Wu, Y.: Marine mixed layer height detection using ship-borne coherent Doppler wind lidar based on constant turbulence threshold, Remote Sensing, 14, 745, 10.3390/rs14030745, 2022.

Wang, L., Qiang, W., Xia, H., Wei, T., Yuan, J., and Jiang, P.: Robust solution for boundary layer height detections with coherent doppler wind lidar, Advances in Atmospheric Sciences, 38, 1920-1928, 10.1007/s00376-021-1068-0, 2021.

Wang, M., Xu, X., Xu, H., Lenschow, D. H., Zhou, M., Zhang, J., and Wang, Y.: Features of the deep atmospheric boundary layer over the Taklimakan Desert in the summertime and its influence on regional circulation, Journal of Geophysical Research: Atmospheres, 124, 12755-12772, 10.1029/2019JD030714, 2019.

Wang, M. Z., Lu, H., Ming, H., and Zhang, J.: Vertical structure of summer clear-sky atmospheric boundary layer over the hinterland and southern margin of Taklamakan Desert, Meteorological Applications, 23, 10.1002/met.1568, 2016.

Wang, T., Han, Y., Huang, J., Sun, M., Jian, B., Huang, Z., and Yan, H.: Climatology of Dust-Forced Radiative Heating Over the Tibetan Plateau and Its Surroundings, Journal of Geophysical Research: Atmospheres, 125, 1-14, 10.1029/2020JD032942, 2020.

Washington, R., Todd, M. C., Engelstaedter, S., M'bainayel, S., and Mitchell, F.: Dust and the low-level circulation over the Bodélé Depression, Chad: Observations from BoDEx 2005, Journal of Geophysical Research, 111, D03201, 10.1029/2005JD006502, 2006.

Wexler, H.: A Boundary Layer Interpretation of the Low-level Jet, Tellus A, 13, 368-378, 10.1111/J.2153-3490.1961.TB00098.X, 1961.

https://doi.org/10.5194/egusphere-2024-1010
Preprint. Discussion started: 15 May 2024

Wu, Wu, G., Guoxiong, Liu, Liu, Y., Yimin, Wang, Wang, T., Tongmei, Wan, Rj, Rijin, Liu, X.-d., Li, Li, W., Weiping, Zz, Zaizhi, Zhang, Zhang, Q., Qiong, Duan, Duan, A., Anmin, Liang, Xy, and Xiaoyun: The Influence of Mechanical and Thermal Forcing by the Tibetan Plateau on Asian Climate, Journal of Hydrometeorology, 8, 770-789, 10.1175/JHM609.1, 2007.

Wu, G., He, B., Duan, A., Liu, Y., and Yu, W.: Formation and variation of the atmospheric heat source over the Tibetan Plateau and its climate effects, Advances in Atmospheric Sciences, 34, 1169-1184, 10.1007/s00376-017-7014-5, 2017.

Wu, G., Liu, Y., He, B., Bao, Q., Duan, A., and Jin, F. F.: Thermal Controls on the Asian Summer Monsoon, Scientific Reports, 2, 1-6, 10.1038/srep00404, 2012.

Wu, K., Wei, T., Yuan, J., Xia, H., Huang, X., Lu, G., Zhang, Y., Liu, F., Zhu, B., and Ding, W.: Thundercloud structures detected and analyzed based on coherent Doppler wind lidar, Atmospheric Measurement Techniques Discussions, 2023, 1-22, 10.5194/amt-2023-73, 2023.

Wu, Y.-P., Feng, G.-L., and Li, B.-L.: Interactions of multiple atmospheric circulation drive the drought in Tarim River Basin, Scientific Reports, 6, 26470, 10.1038/srep26470, 2016.

Xiao, F., Zhou, C., and Liao, Y.: Dust storms evolution in Taklimakan Desert and its correlation with climatic parameters, Journal of Geographical Sciences, 18, 415-424, 10.1007/s11442-008-0415-8, 2008.

Yang, X., Shen, S., Yang, F., He, Q., Ali, M., Huo, W., and Liu, X.: Spatial and temporal variations of blowing dust events in the Taklimakan Desert, Theoretical and Applied Climatology, 125, 669-677, 10.1007/s00704-015-1537-4, 2016.

Yang, X., He, Q., Matimin, A., Yang, F., Huo, W., Liu, X., Zhao, T., and Shen, S.: Threshold velocity for saltation activity in the Taklimakan Desert, Pure and Applied Geophysics, 174, 4459-4470, 10.1007/s00024-017-1644-5, 2017.

Yuan, J., Xia, H., Wei, T., Wang, L., Yue, B., and Wu, Y.: Identifying cloud, precipitation, windshear, and turbulence by deep analysis of the power spectrum of coherent Doppler wind lidar, Optics Express, 28, 37406-37418, 10.1364/OE.412809, 2020.

Yuan, J., Wu, K., Wei, T., Wang, L., Shu, Z., Yang, Y., and Xia, H.: Cloud seeding evidenced by coherent Doppler wind Lidar, Remote Sensing, 13, 3815, 10.3390/rs13193815, 2021.

Zhang, H., Zhang, X., Li, Q., Cai, X., Fan, S., Song, Y., Hu, F., Che, H., Quan, J., Kang, L., and Zhu, T.: Research Progress on Estimation of the Atmospheric Boundary Layer Height, Journal of Meteorological Research, 34, 482-498, 10.1007/s13351-020-9910-3, 2020.

Zhang, L., Zhang, H., Li, Q., Wei, W., Cai, X., Song, Y., Mamtimin, A., Wang, M., Yang, F., and Wang, Y.: Turbulent mechanisms for the deep convective boundary layer in the Taklimakan Desert, Geophysical Research Letters, 49, e2022GL099447, 10.1029/2022GL099447, 2022.

Zhang, Q., Cao, X., Wei, G., and Huang, R.: Observation and Study of Land Surface Parameters over Gobi in Typical Arid Region, Advances in Atmospheric Sciences, 19, 121-135, 10.1007/s00376-002-0039-3, 2002.

Zhang, Q., Zhang, J., Qiao, J., and Wang, S.: Relationship of atmospheric boundary layer depth with thermodynamic processes at the land surface in arid regions of China, Science China Earth Sciences, 54, 1586-1594, 10.1007/S11430-011-4207-0, 2011.

https://doi.org/10.5194/egusphere-2024-1010
Preprint. Discussion started: 15 May 2024

Zhang, W., Guo, J., Miao, Y., Liu, H., Song, Y., Fang, Z., He, J., Lou, M., Yan, Y., Li, Y., and Zhai, P.: On the Summertime Planetary Boundary Layer with Different Thermodynamic Stability in China: A Radiosonde Perspective, Journal of Climate, 31, 1451-1465, 10.1175/JCLI-D-17-0231.1, 2017.

Zhang, Y., Seidel, D. J., and Zhang, S.: Trends in Planetary Boundary Layer Height over Europe, Journal of Climate, 26, 10071-10076, 10.1175/JCLI-D-13-00108.1, 2013.

Zhang, Y., Wu, Y., and Xia, H.: Spatial resolution enhancement of coherent Doppler wind lidar using differential correlation pair technique, Optics Letters, 46, 5550-5553, 10.1109/jlt.2022.3160294, 2021.

Zhou, C., Yang, F., Mamtimin, A., Huo, W., Liu, X., He, Q., Zhang, J., and Yang, X.: Wind erosion events at different wind speed levels in the Tarim Basin, Geomorphology, 369, 107386, 10.1016/j.geomorph.2020.107386, 2020.

Zhou, C., Liu, Y., He, Q., Zhong, X., Zhu, Q., Yang, F., Huo, W., Mamtimin, A., Yang, X., and Wang, Y.: Dust characteristics observed by unmanned aerial vehicle over the Taklimakan Desert, Remote Sensing, 14, 990, 10.3390/rs14040990, 2022.